Support information

Anisotropic, low-tortuosity, ultra-thick red P@C-Wood electrodes for sodium-ion batteries

Longfei Han, Junling Wang, Xiaowei Mu, Can Liao, Wei Cai, Zhixin Zhao, Yongchun Kan,* Weiyi Xing* and Yuan Hu

State Key Laboratory of Fire Science, CAS Key Laboratory of Soft Matter Chemistry, University of Science and Technology of China, Hefei 230026, China

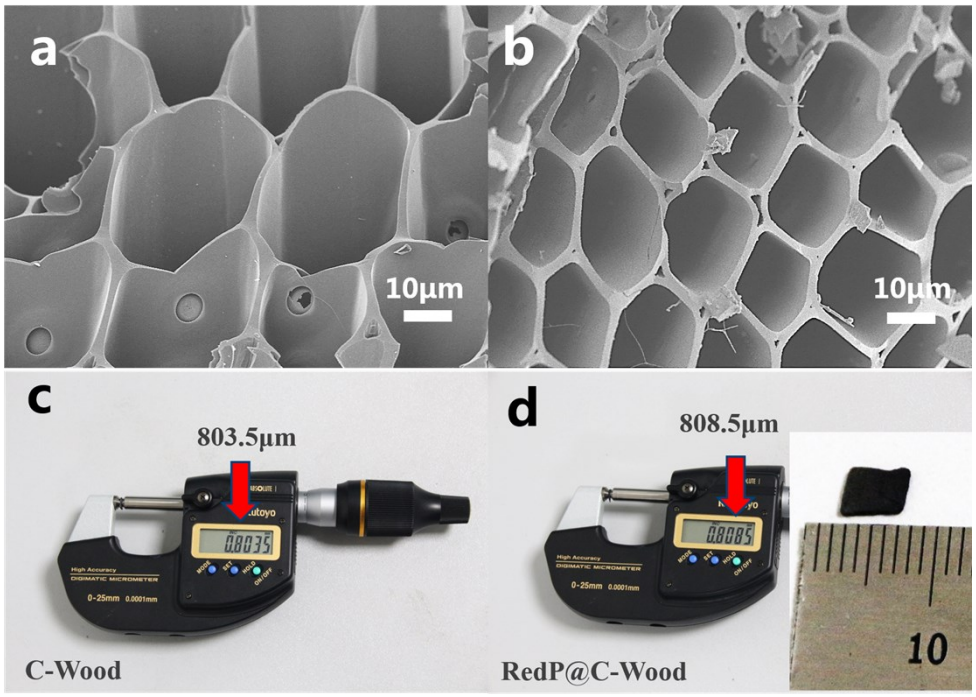

Fig. S1 A low-magnification SEM image of (a) the C-Wood and (b) red P@C-Wood. The thickness of (c) the C-Wood and (d) red P@C-Wood (the size of red P@C-Wood is about 5 mm × 5 mm × 0.8 mm).

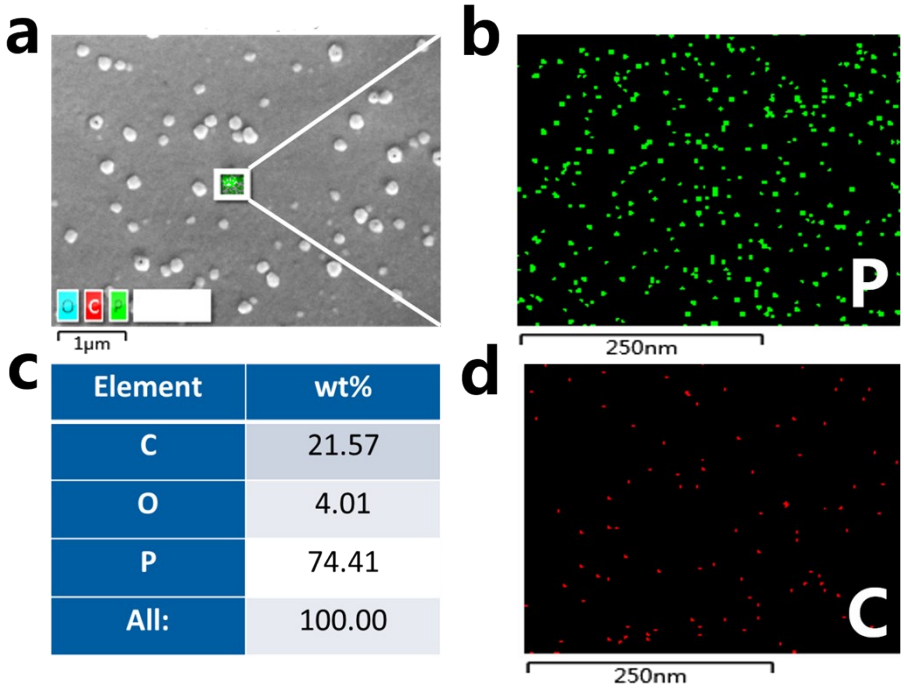

Element	wt%
C	21.57
O	4.01
P	74.41
All:	100.00

Fig. S2 SEM and EDS elemental mapping of red P nanoparticles.

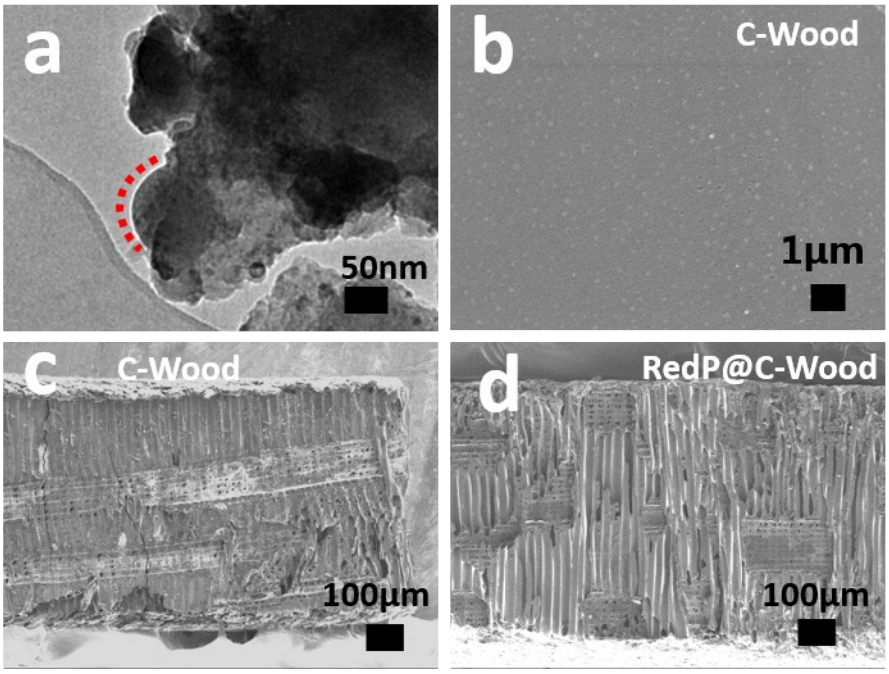

Fig. S3 (a) TEM image of the red P@C-Wood. (b) A high-magnification SEM image of the C-Wood. Photo images of the thickness of the C-Wood (c) and (d) red P@C-Wood

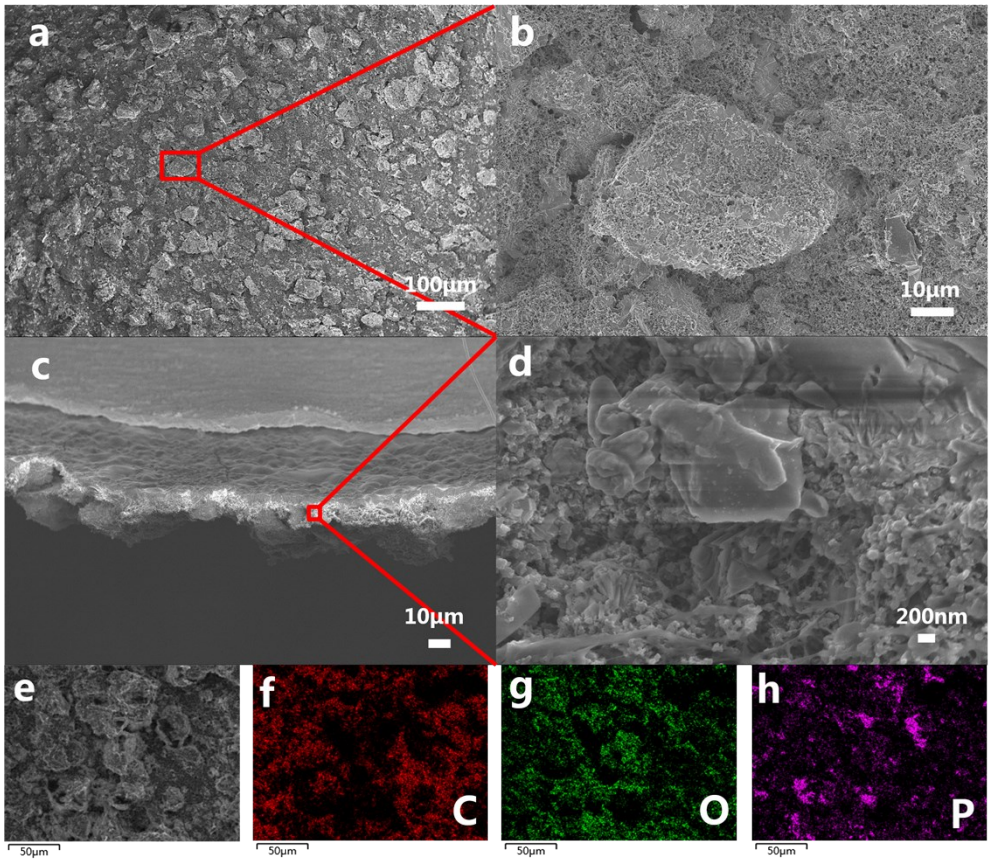

Fig. S4 Morphological and structural characterizations of the red P electrode at different states. The top view (a), (b), (e) and cross-section view (c), (d) of red P electrode, respectively. (f-h) Corresponding C, O, and P elemental mapping images of the red P electrode.

For the comparison, the red phosphorus is mixed with acetylene black and poly(vinylidene fluoride) (PVDF) to make a homogeneous slurry(the ratio was 8:1:1). Then the slurry is cast onto copper foil using a doctor blade, followed by drying in a vacuum 12 h at 60 °C. The mass loading of the electrodes is about 1.0 mg cm^{-2}.

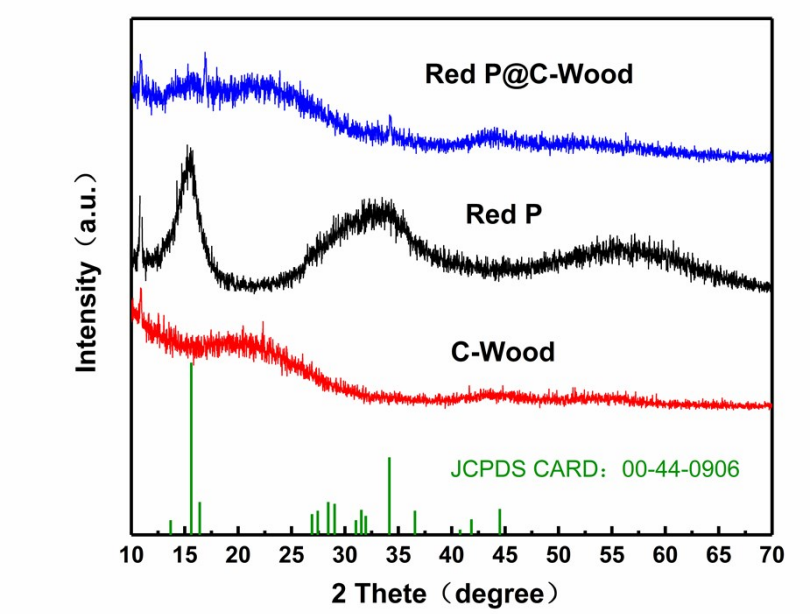

Fig. S5 XRD patterns of the C-Wood, red P and red P@C-Wood.

Table. S1 The red P loading of pure red P electrode and red P@C-Wood electrode.

Sample	Red P loading (wt%)	Red P loading (mg cm^{-2})
Red P electrode	**15**	**1.522**
Red P@C-Wood	**30**	**8.371**

For the pure red P electrode, the red phosphorus loading (wt%) is calculated based on 15% with half of a 12.5 μm copper current collector, red phosphorus, acetylene black and PVDF.

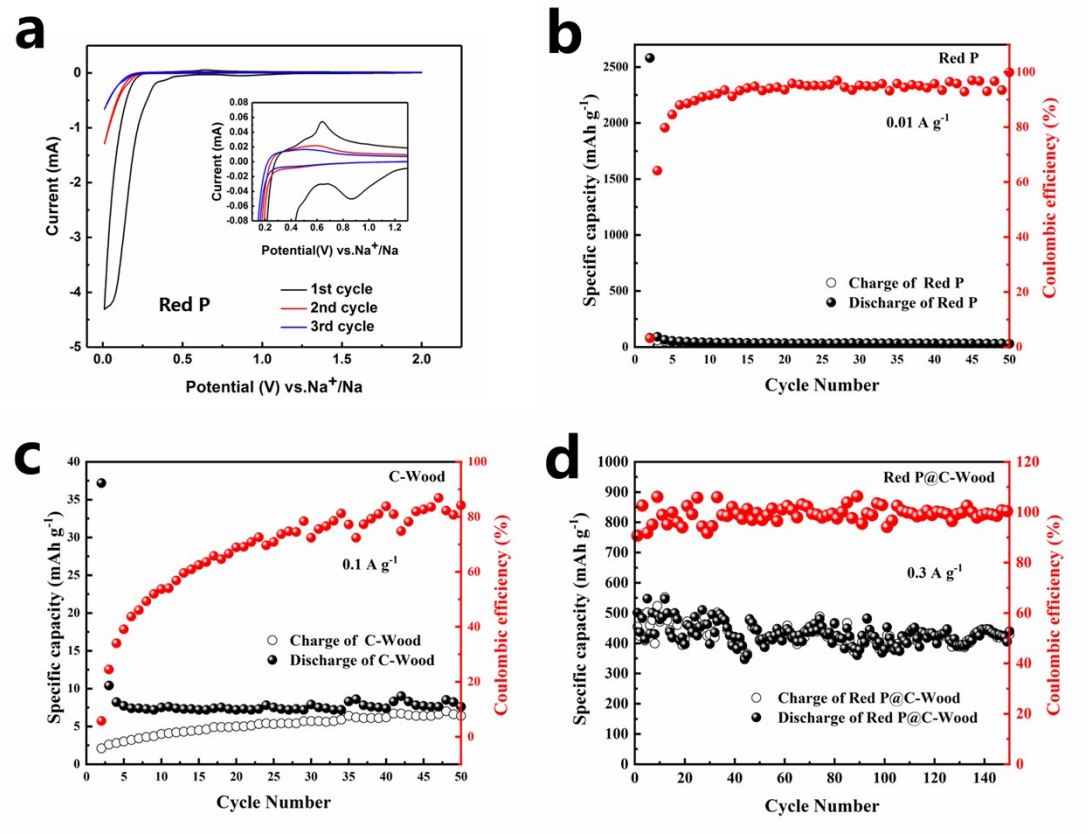

Fig. S6 (a) Cyclic voltammetry of pure red P electrode at the potential window between 0.01 and 2.0 V versus Na/Na^+ with a scan rate of 0.1 mV s^{-1}; (b) cycling properties of the red P electrode at 0.01 A g^{-1}; (c) cycling properties of the pure red P electrode at 0.1 A g^{-1}; (d) cycling properties of red P@C-Wood electrode at 0.3 A g^{-1}.

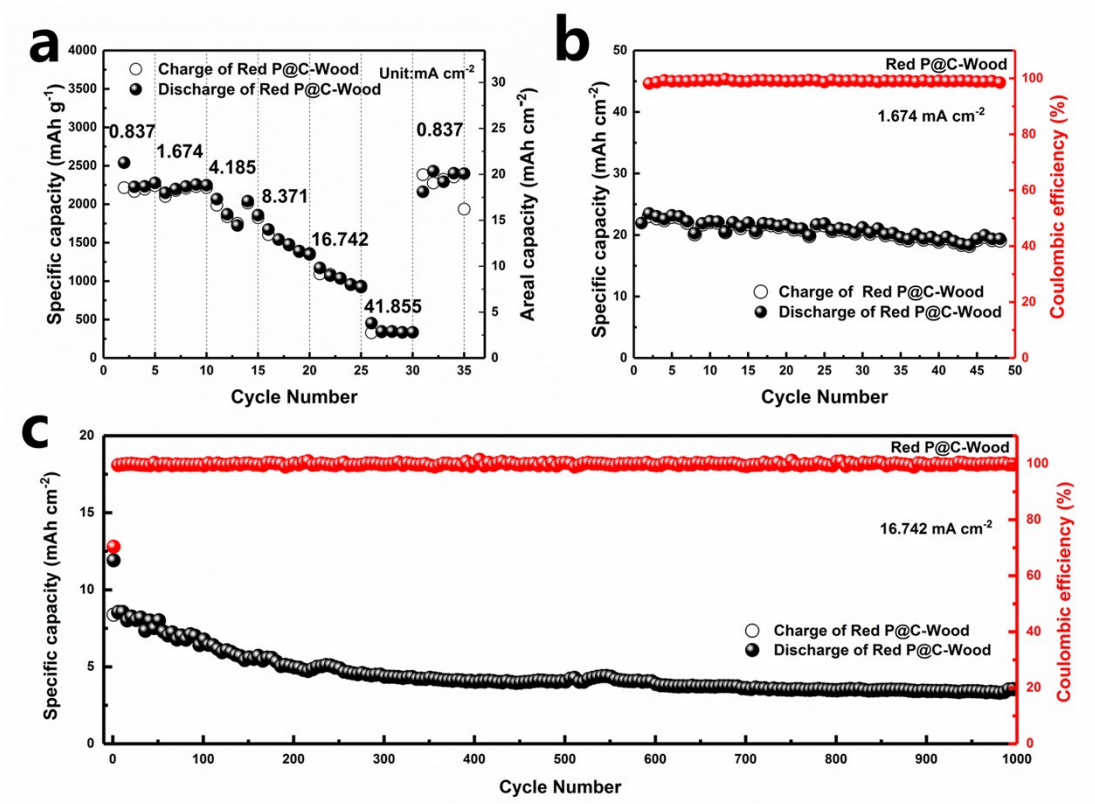

Fig. S7 (a) Rate capabilities and (b) cycling properties of the red P@C-Wood electrode at 1.674 mA cm^{-2}. (c) Long cycling performance of the red P@C-Wood electrode at 16.742 mA cm^{-2}.

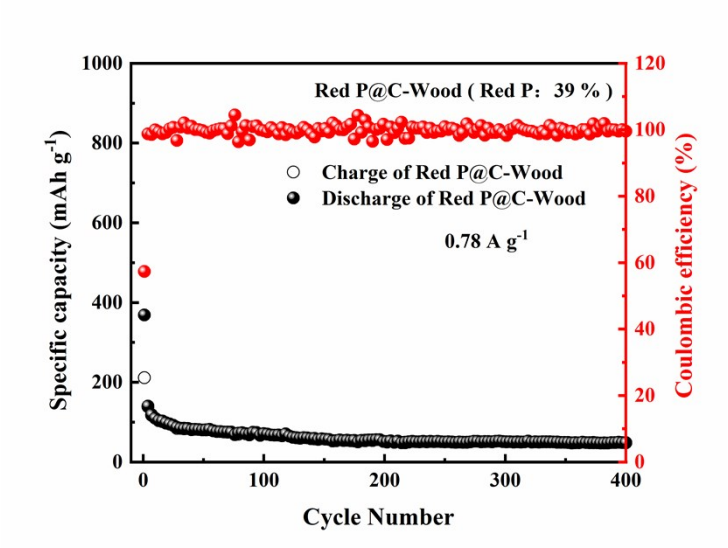

Fig. S8 Cycling properties of the red P@C-Wood electrode at 0.78 A g^{-1} based on red P@C-Wood, red P content is about 39 wt% (Red P@C-Wood = 100:50)

Table. S2 The elemental analyzer data of wood (wt%).

Materials	C	H	N	S	O
Wood	47.21	6.62	0.09	0.88	45.69

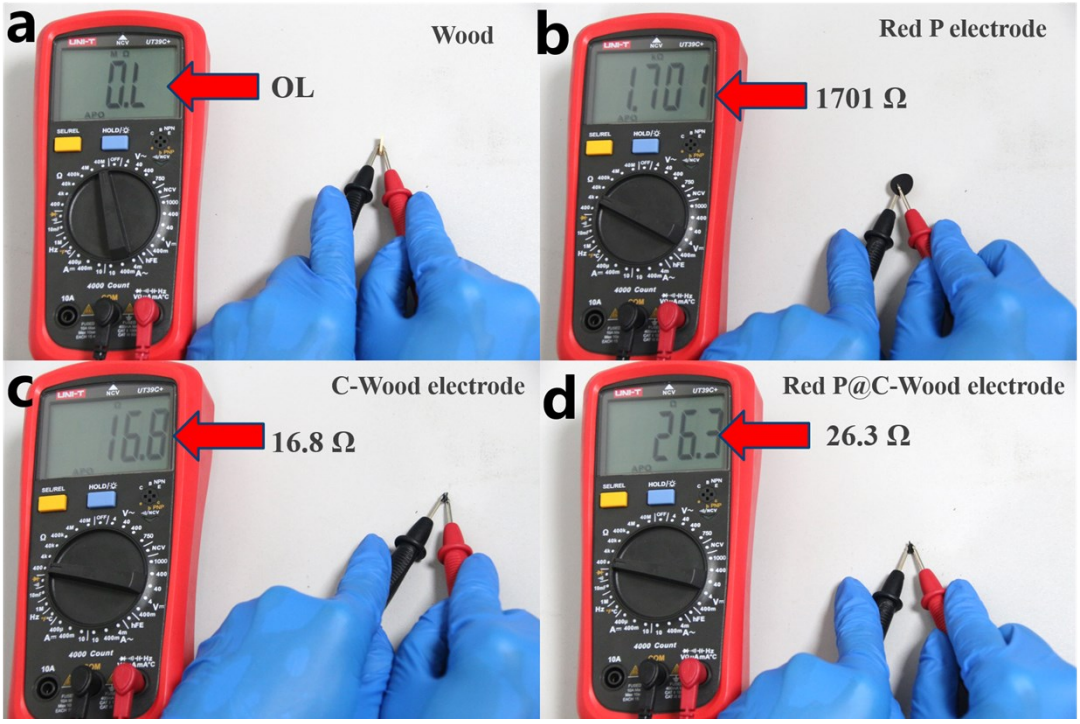

Fig. S9 Evaluation of resistance using a multimeter.

Table. S3 The resistance of different materials.

Materials	Resistance
Wood	≥ 40 M Ω
Red P electrode	1701 Ω
C-Wood	16.8 Ω
Red P@C-Wood	26.3 Ω

Table. S4 Comparison with red P based anodes for SIBs in literatures.

Materials	P content in composites	P content in whole electrode[a]	Mass loading of P (mg/cm^{-2})	Reversible capacity (based on P)	Reversible capacity (based on P/C composites)	Gravimetric capacity (based on whole electrode)[a]	Gravimetric capacity (based on whole electrode)[a]	Reference
Red P@C-Wood	30 wt%	30 wt%	8.4	2239.8 mAh g^{-1} at 0.2 A g^{-1}	791.8 mAh g^{-1} at 0.06 A g^{-1}	791.8 mAh g^{-1} at 0.06 A g^{-1}	18.8 mAh cm^{-2} at 1.67 mA cm^{-2}	This work
				1057.8 mAh g^{-1} at 2.0 A g^{-1}	320.5 mAh g^{-1} at 0.6 A g^{-1}	320.5 mAh g^{-1} at 0.6 A g^{-1}	8.9 mAh cm^{-2} at 16.7 mA cm^{-2}	This work
P/CNTs@rGO	70 wt%	70 wt%	1.5	2113 mAh g^{-1} at 0.52 A g^{-1}	1479 mAh g^{-1} at 0.42 A g^{-1}	1479 mAh g^{-1} at 0.42 A g^{-1}	3.2 mAh cm^{-2} at 0.78 mA cm^{-2}	1
P@N-MPC composites	22.6 wt%	5.2 wt%	~ 0.34	2522.1 mAh g^{-1} at 4.4 A g^{-1}	570 mAh g^{-1} at 1.0 A g^{-1}	131.5 mAh g^{-1} at 0.1 A g^{-1}	0.85 mAh cm^{-2} at 1.5 mA cm^{-2}	2
P/CNTs@rGO	70 wt%	10.6 wt%	~ 2.2	2007.1 mAh g^{-1} at 0.74 A g^{-1}	1405 mAh g^{-1} at 0.52 A g^{-1}	211.9 mAh g^{-1} at 0.52 A g^{-1}	4.4 mAh cm^{-2} at 1.6 mA cm^{-2}	3
P@C-GO/ MOF-5	~44.5 wt%	8.5 wt%	~0.45	1865.2 mAh g^{-1} at 4.5 A g^{-1}	830 mAh g^{-1} at 2.0 A g^{-1}	158.4 mAh g^{-1} at 0.17 A g^{-1}	0.84 mAh cm^{-2} at 2.0 mA cm^{-2}	4
RP/rGO	57.9 wt%	57.9 wt%	~ 0.87	1550 mAh g^{-1} at 1 A g^{-1}	897.4 mAh g^{-1} at 0.58 A g^{-1}	897.4 mAh g^{-1} at 0.58 A g^{-1}	1.35 mAh cm^{-2} at 0.87 mA cm^{-2}	5

P@AC@PPy	52 wt%	10 wt%	0.62	800 mAh g^{-1} at 0.1 A g^{-1}	416 mAh g^{-1} at 0.05 A g^{-1}	80 mAh g^{-1} at 0.01 A g^{-1}	0.5 mAh cm^{-2} at 0.06 mA cm^{-2}	6
RH-3-1-RP/CS	60 wt%	23.4 wt%	3	1027 mAh g^{-1} at 4 A g^{-1}	616.2 mAh g^{-1} at 2.4 A g^{-1}	240.3 mAh g^{-1} at 0.9 A g^{-1}	3.1 mAh cm^{-2} at 12 mA cm^{-2}	7
NRP−rGO	56.3 wt%	18 wt%	0.39	1176 mAh g^{-1} at 3.6 A g^{-1}	662 mAh g^{-1} at 2 A g^{-1}	211.7 mAh g^{-1} at 0.65 A g^{-1}	0.46 mAh cm^{-2} at 1.4 mA cm^{-2}	8
S-P/ rGO	45.6 wt%	12 wt%	0.9	1364.1 mAh g^{-1} at 2.6 A g^{-1}	622 mAh g^{-1} at 1.2 A g^{-1}	163.7 mAh g^{-1} at 0.31 A g^{-1}	1.2 mAh cm^{-2} at 2.3 mA cm^{-2}	9

a. The calculated gravimetric capacity of whole electrode is based on the mass of active materials, binder, conductive additive and current collectors (Capacity $_{electrode}$ = capacity $_{active\ materials}$/ (mass $_{active\ materials}$ + mass $_{binder}$ + mass $_{conductive\ additive}$ + mass $_{current\ collectors}$)). The current density of whole electrode is according to the reported current density based on the P multiplying by the weight ratio of P in composites, such as : Current density $_{electrode}$ = Current density $_{active\ materials}$ × weight ratio $_{active\ materials}$. All the loading mass is according to the reported value in references.

References

1. J. Zhou, Z. Jiang, S. Niu, S. Zhu, J. Zhou, Y. Zhu, J. Liang, D. Han, K. Xu, L. Zhu, X. Liu, G. Wang and Y. Qian, *Chem*, 2018, **4**, 372-385.
2. W. Li, S. Hu, X. Luo, Z. Li, X. Sun, M. Li, F. Liu and Y. Yu, *Adv Mater*, 2017, **29**, 1605820.
3. S. Liu, J. K. Feng, X. F. Bian, J. Liu, H. Xu and Y. L. An, *Energ Environ Sci*, 2017, **10**, 1222-1233.
4. Y. Wu, Z. Liu, X. Zhong, X. Cheng, Z. Fan and Y. Yu, *Small*, 2018, **14**, 1703472.
5. Y. H. Liu, A. Y. Zhang, C. F. Shen, Q. Z. Liu, J. S. Cai, X. Cao and C. W. Zhou, *Nano Res*, 2018, **11**, 3780-3790.
6. K. Fang, D. Liu, X. Y. Xiang, X. X. Zhu, H. L. Tang, D. Y. Qu, Z. Z. Xie, J. S. Li and D. Y. Qu, *Nano Energy*, 2020, **69**, 104451.

7. H. L. Jin, H. Lu, W. Y. Wu, S. Q. Chen, T. C. Liu, X. X. Bi, W. N. Xie, X. Chen, K. Q. Yang, J. Li, A. L. Liu, Y. Lei, J. C. Wang, S. Wang and J. Lu, *Nano Energy*, 2020, **70**, 104569.
8. W. L. Liu, S. L. Ju and X. B. Yu, *Acs Nano*, 2020, **14**, 974-984.
9. J. B. Zhou, X. J. Liu, L. Q. Zhu, S. W. Niu, J. Y. Cai, X. S. Zheng, J. Ye, Y. Lin, L. Zheng, Z. X. Zhu, D. Sun, Z. Lu, Y. P. Zang, Y. S. Wu, J. X. Xiao, Q. Liu, Y. C. Zhu, G. M. Wang and Y. T. Qian, *Chem*, 2020, **6**, 221-233.